Available online at www.sciencedirect.com

ScienceDirect

IFAC Papers Online CONFERENCE PAPER ARCHIVE

IFAC PapersOnLine 53-2 (2020) 9144–9149

Active vibration isolation by model reference adaptive control

W.B.J. Hakvoort * **G.J. Boerrigter** *,** **M.A. Beijen** **

* *University of Twente, Faculty of Engineering Technology, Department of Mechanics of Solids, Surfaces and Systems, PO Box 217, 7500 AE Enschede, The Netherlands (e-mail: w.b.j.hakvoort@utwente.nl)*
** *DEMCON Advanced Mechatronics, Institutenweg 25, 7521 PH Enschede, The Netherlands*

Abstract: This paper proposes model reference adaptive control (MRAC) to actively isolate payloads from floor vibrations and direct disturbance forces. Adaptive feedforward control is used to counteract measured disturbances, whereas an adaptive feedback controller suppresses unmeasured disturbances using skyhook damping. In the considered rigid single degree of freedom system, the ideal controller gains only depend on the stiffness and damping properties of the suspension. The MRAC strategy is validated experimentally on a hard mounted vibration isolation system. Attenuation of acceleration levels beyond $-40\,\mathrm{dB}$ are obtained in a wide frequency band $5-100\,\mathrm{Hz}$ and the root-mean-square (RMS) acceleration in the frequency region of interest $(0.1-100\,\mathrm{Hz})$ is reduced 32 times with respect to passive isolation.

Keywords: Model reference adaptive control, MRAC, active vibration isolation, high-precision mechatronics, disturbance feedforward control

1. INTRODUCTION

Many high-precision machines need isolation from floor vibrations and disturbance forces acting directly on the machine (Fuller et al. (1996); Heertjes et al. (2005); Preumont et al. (2007)). Examples include wafer steppers and scanners, atomic force microscopes, and laser communication systems. Passive vibration isolation (Rivin (2003)) benefits from a high payload mass, while the support stiffness introduces a trade-off between rejection of floor vibrations (soft mount) or rejection of direct disturbance forces (hard mount). Active vibration isolation control (AVIC) can circumvent this trade-off and requires less payload mass for effective vibration isolation.

A common AVIC strategy is skyhook damping (Karnopp, 1995), which uses absolute velocity feedback to add artificial damping. More advanced feedback control methods specify the dynamic behaviour by a reference model or manifold and match the actual dynamics to the reference model using adaptive algorithms. Examples include adaptive sliding-mode control (ASMC) (Alleyne and Hedrick, 1995; Wang and Sinha, 1997) and model-reaching adaptive control (Zuo et al., 2005). Alternative AVIC strategies use feedforward of a measured disturbance source for AVIC, mostly in combination with adaptive self-tuning filters (van der Poel et al., 2007; Beijen et al., 2018a). This strategy leads to better signal-to-noise (SNR) ratios and preserved stability properties compared to feedback control. In some cases feedback is added to improve performance, but the controller parameters are not updated in the adaptation law. Moreover, existing adaptation laws require prior knowledge of the so-called feedforward transmission path (Wesselink and Berkhoff, 2008), which is the transfer function between the control signal and the payload acceleration.

Adaptive feedforward and feedback AVIC have thus been proposed, but a systematic method to simultaneously design and adapt feedforward and feedback control is lacking. Therefore, the first and main contribution of this paper is the formulation of the vibration isolation problem in the *model reference adaptive control* (MRAC) context. In this context, the desired plant behaviour is described by a stable reference model, which is driven by a reference input (Landau, 1974; Åström and Wittenmark, 2013). The proposed reference model has zero response to measured disturbances (feedforward), while it has high damping to counteract unmeasured disturbances (feedback). This provides a systematic method to simultaneously design feedforward and feedback for wide-band disturbance rejection. The feedforward and feedback control are simultaneously adapted with state stability and parameter boundedness guaranteed by Lyapunov's stability theory (Khalil and Grizzle, 2002). Moreover, it is shown that the MRAC formulation does not require prior knowledge of the feedforward transmission path. The second contribution is a method to circumvent the experimentally observed non persistent excitation of the feedback gains, based on physics considerations. The third contribution is the experimental validation of the wide-band vibration isolation on an experimental hard-mounted system.

The structure of this paper is as follows. A description of the vibration isolation control objective, the MRAC setting and the proposed reference model are presented in Sec. 2. Sec. 3 considers the MRAC design. The design is validated with experimental results as presented in Sec. 4. The conclusions are given in Sec. 5.

10.1016/j.ifacol.2020.12.2157

2. PROBLEM DEFINITION

A simplified model of a vibration isolation system is shown in Fig. 1. The payload mass m is suspended to the floor by means of a spring with stiffness k and viscous damper d. $F_s(t)$ and $F_d(t)$ are respectively the measured and unmeasured direct disturbance forces, which are induced by, e.g, acoustics, vibrating cables or accelerating stages. $F_a(t)$ is the control action for active vibration isolation of the payload. The absolute positions of the floor and payload are represented by $x_0(t)$ and $x_1(t)$ respectively. Acceleration sensors measure the related accelerations of the floor and payload, denoted by $a_0(t)$ and $a_1(t)$. The state-space representation of the plant dynamics is

$$\dot{\boldsymbol{x}}_p(t) = \boldsymbol{A}_p\boldsymbol{x}_p(t) + \boldsymbol{B}_p u(t) + \boldsymbol{E}_p\boldsymbol{r}(t) + \boldsymbol{G}_p w(t)\,, \qquad (1)$$

with

$$\begin{aligned} \boldsymbol{x}_p(t) &= [x_1(t)\ \dot{x}_1(t)]^T\,, \quad u(t) = F_a(t)\,,\\ \boldsymbol{r}(t) &= [x_0(t)\ \dot{x}_0(t)\ F_s(t)]^T\,, \quad w(t) = F_d(t)\,,\\ \boldsymbol{A}_p &= \begin{bmatrix} 0 & 1 \\ -k/m & -d/m \end{bmatrix}\,,\\ \boldsymbol{B}_p = \boldsymbol{G}_p &= \begin{bmatrix} 0 \\ 1/m \end{bmatrix}\,, \quad \boldsymbol{E}_p = \begin{bmatrix} 0 & 0 & 0 \\ k/m & d/m & 1/m \end{bmatrix}\,, \end{aligned} \qquad (2)$$

with plant state vector $\boldsymbol{x}_p(t)$, control action $u(t)$, unknown disturbances $w(t)$ and the reference vector $\boldsymbol{r}(t)$, which contains the measured disturbances.

The objective of vibration isolation is to reduce the payload accelerations $a_1(t)$ by controlling the actuator force $F_a(t)$. This is realised through feedforward control from direct measurement of the floor acceleration $a_0(t)$ and the measured disturbance force $F_s(t)$ and feedback control using the measured payload acceleration $a_1(t)$ to compensate for the unmeasured disturbance force $F_d(t)$. The vibration isolation performance is specified by the *transmissibility* $\mathcal{T}$ and *compliances* $\mathcal{C}_s$ and $\mathcal{C}_d$, which are defined as the controlled transfer functions from respectively the floor acceleration, measured disturbance and unmeasured disturbance forces to the payload acceleration.

2.1 MRAC structure

In this paper a *direct* MRAC system with *state feedback* is proposed for vibration isolation (Landau, 1974; Åström and Wittenmark, 2013). The structure is shown in Fig. 2. In MRAC, the control action $u(t) \in \mathbb{R}$ is such that all signals in the closed-loop plant are bounded, and states $\boldsymbol{x}_p(t) \in \mathbb{R}^2$ track states $\boldsymbol{x}_m(t) \in \mathbb{R}^2$ of a specified reference model driven by the measured disturbances $\boldsymbol{r}(t)$. The reference model is discussed in Sec. 2.2. MRAC requires the reference model to be of the same system order as the plant model, and all signals in $\boldsymbol{x}_p(t)$ and $\boldsymbol{r}(t)$ to be measured or estimated. Since $w(t)$ contains unmeasured disturbance force by definition, it cannot be taken into account in the reference model. $\boldsymbol{K}_x \in \mathbb{R}^{1\times 2}$ and $\boldsymbol{K}_r \in \mathbb{R}^{1\times 3}$ are matrices containing the feedback and feedforward controller gains. NSF denotes a residual noise shaping filter, which is discussed in Sec. 3.2.

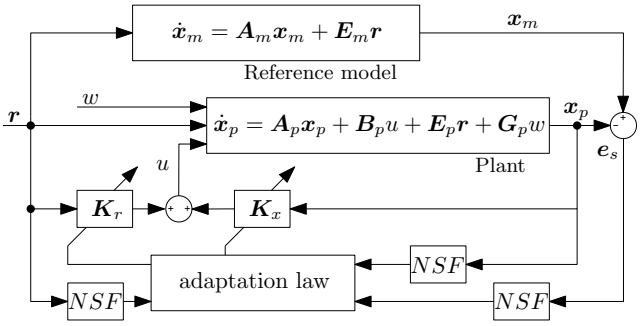

Fig. 2. Direct MRAC structure with state feedback for the considered vibration isolation setting.

2.2 Reference model

The reference model specifies the desired behaviour of the controlled system and thereby the desired transmissibility $\mathcal{T}$ and the compliances $\mathcal{C}_s$ and $\mathcal{C}_d$. The reference model should be of the same order as the actual dynamics to allow state tracking. A general second-order reference model is shown in Fig. 3. Payload m_m with position $x_{m,1}(t)$ is connected to the vibrating floor $x_0(t)$ through spring k_m and viscous damper d_m. Measured direct disturbance force $F_s(t)$ acts on m_m with multiplier f_m. The unmeasured disturbance $w(t) = F_d$ is not included, since the response of this disturbances cannot be determined. Furthermore, a hypothetical (fixed) 'sky' is added to which m_m is attached by means of skyhook spring k_s and skyhook damper d_s. The state space reference of the plant dynamics is

$$\dot{\boldsymbol{x}}_m(t) = \boldsymbol{A}_m\boldsymbol{x}_m(t) + \boldsymbol{E}_m\boldsymbol{r}(t)\,, \qquad (3)$$

with

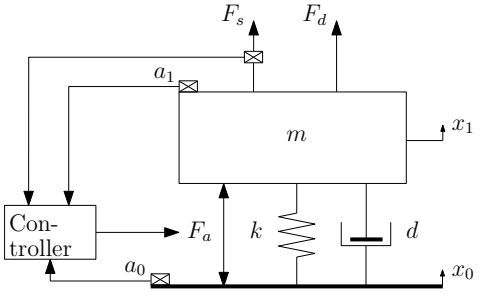

Fig. 1. Model of active vibration isolation system.

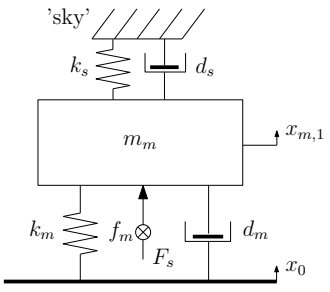

Fig. 3. Proposed 'skyhook' reference model.

$$\begin{aligned}\boldsymbol{x}_m(t) &= [x_{m,1}(t)\ \dot{x}_{m,1}(t)]^T\ ,\\ \boldsymbol{A}_m &= \begin{bmatrix} 0 & 1 \\ -(k_m+k_s)/m_m & -(d_m+d_s)/m_m \end{bmatrix}, \\ \boldsymbol{E}_m &= \begin{bmatrix} 0 & 0 & 0 \\ k_m/m_m & d_m/m_m & f_m/m_m \end{bmatrix}.\end{aligned} \tag{4}$$

The desired (closed-loop) transmissibility and compliance are defined by the following parameter selection for the reference model.

Proposition 1. Taking $d_m = 0$, $k_m = 0$ and $f_m = 0$ makes all elements of E_m zero and thereby the transmissibility $\mathcal{T}$ and compliance $\mathcal{C}_s$ are zero. This isolates payload m from all measured disturbances. The absence of any force acting on the payload results in $\boldsymbol{x}_m(t) = 0$, which means the payload is in rest. As a result, the differential equation (3) does not have to be solved online, which reduces computational cost. Furthermore, $\boldsymbol{x}_m(t) = 0$ holds, regardless of the remaining parameters k_s, d_s and m_m. Thereby, any finite parameter value can be assigned to these parameters, even the (unknown) plant parameters.

The parameters from proposition 1 eliminate the effect of the measured disturbances, i.e., $\mathcal{T}$ and $\mathcal{C}_s$ are zero, which effectively introduces disturbance feedforward control in MRAC. The remaining parameters k_s, d_s and m_m define the compliance $\mathcal{C}_d$, effectively introducing skyhook damping and stiffness. This compliance is low by the high passive stiffness of the hard mounts in combination with a high skyhook damping provided by the feedback controller. In view of Proposition 1, this can be realised by the selection of unknown parameters $m_m = m$ and $k_s = k$, while adding a defined skyhook damping d_s.

3. DESIGN OF MRAC

This section considers the model matching controller and the adaptation law for the proposed MRAC. After this, some implementation issues and related performance limitations are discussed.

3.1 Model matching

The controller with feedforward of the measured disturbances and state-feedback reads

$$u(t) = \boldsymbol{K}_x^* \boldsymbol{x}_p(t) + \boldsymbol{K}_r^* \boldsymbol{r}(t)\,, \tag{5}$$

where $\boldsymbol{K}_x^* \in \mathbb{R}^{1\times 2}$, $\boldsymbol{K}_r^* \in \mathbb{R}^{1\times 3}$ are the ideal control gain matrices of the feedback and feedforward path, respectively. These should ensure matching of the plant and reference model. Upon substitution of (5) in (1), the following closed-loop plant is obtained:

$$\dot{\boldsymbol{x}}_p(t) = (\boldsymbol{A}_p + \boldsymbol{B}_p \boldsymbol{K}_x^*)\, \boldsymbol{x}_p(t) + (\boldsymbol{E}_p + \boldsymbol{B}_p \boldsymbol{K}_r^*)\, \boldsymbol{r}(t)\,. \tag{6}$$

It can be derived straightforwardly, that the closed-loop plant (6) matches the reference model (3) with the following ideal controller gains

$$\boldsymbol{K}_x^* = [0\,, -d_s + d\,,\ 0\,,\ 0]\ , \tag{7a}$$

$$\boldsymbol{K}_r^* = [-k\,,\ -d\,,\ -1]\ . \tag{7b}$$

The feedback control gains only includes a negative feedback term equal to the reference model's damping minus the real damping to obtain the reference skyhook damping. No stiffness term is obtained, because the stiffness of the reference model is taken equal to the real stiffness. It can be shown that the dynamics in (4) with the feedback in (7) is positive real (sensor and actuator are collocated), providing high stability margins to cope with parasitic dynamics (see Sec. 3.3). The feedforward control gains for model matching only requires knowledge of the fundamental stiffness and damping properties of the vibration isolator. Furthermore, the disturbance force $F_s(t)$ in $\boldsymbol{r}(t)$ is directly compensated by third element of $\boldsymbol{K}_r^*$ being -1, which requires no knowledge of plant parameters. The first two terms of the feedforward control gains in (7b) are identical to the Wiener solution for disturbance feedforward control obtained in Beijen et al. (2018a).

3.2 Adaptation law

The controller in (5) requires the unknown parameters k and d to calculate the gains in (7) for perfect cancellation of the measured disturbances. Therefore, these gains are obtained though online adaptation. MRAC provides a method to achieve concurrent parameter adaptation and state-tracking. The state tracking error between reference model and plant is defined by $\boldsymbol{e}_s(t) = \boldsymbol{x}_m(t) - \boldsymbol{x}_p(t) \in \mathbb{R}^2$ and the parameter errors are defined as $\hat{\boldsymbol{K}}_x(t) = \boldsymbol{K}_x(t) - \boldsymbol{K}_x^* \in \mathbb{R}^{1\times 2}$, $\hat{\boldsymbol{K}}_r(t) = \boldsymbol{K}_r(t) - \boldsymbol{K}_r^* \in \mathbb{R}^{1\times 3}$.

The adaptation law and convergence analysis are in line with Åström and Wittenmark (2013) and presented without details. The adaptation rule is defined as

$$\begin{aligned}\dot{\hat{\boldsymbol{K}}}_x^T &= \dot{\boldsymbol{K}}_x^T = \boldsymbol{\Gamma}_x \boldsymbol{x}_p \boldsymbol{e}_s^T \bar{\boldsymbol{P}} \mathrm{sgn}(b_p)\,,\\ \dot{\hat{\boldsymbol{K}}}_r^T &= \dot{\boldsymbol{K}}_r^T = \boldsymbol{\Gamma}_r \boldsymbol{r} \boldsymbol{e}_s^T \bar{\boldsymbol{P}} \mathrm{sgn}(b_p)\,,\end{aligned} \tag{8}$$

where $\boldsymbol{\Gamma}_x = \boldsymbol{\Gamma}_x^T > 0 \in \mathbb{R}^{2\times 2}$ and $\boldsymbol{\Gamma}_r = \boldsymbol{\Gamma}_r^T > 0 \in \mathbb{R}^{3\times 3}$ are adaptation gain matrices. $\bar{\boldsymbol{P}}$ is the bottom row of $\boldsymbol{P}$ with $\boldsymbol{P} = \boldsymbol{P}^T > 0 \in \mathbb{R}^{2\times 2}$ satisfying the Lyapunov equation $\boldsymbol{P}\boldsymbol{A}_m + \boldsymbol{A}_m^T \boldsymbol{P} = -\boldsymbol{Q}$ for some $\boldsymbol{Q} = \boldsymbol{Q}^T > 0 \in \mathbb{R}^{2\times 2}$. The variable $b_p \in \mathbb{R}$ is the only non-zero element of $\boldsymbol{B}_p$, which has a positive sign considering (2).

Consider the following Lyapunov function

$$\begin{aligned}\mathcal{V}\left(\boldsymbol{e}_s, \hat{\boldsymbol{K}}_x, \hat{\boldsymbol{K}}_r\right) &= \boldsymbol{e}_s^T \boldsymbol{P} \boldsymbol{e}_s \\ &+ |b_p| \left(\hat{\boldsymbol{K}}_x \boldsymbol{\Gamma}_x^{-1} \hat{\boldsymbol{K}}_x^T\right) + |b_p| \left(\hat{\boldsymbol{K}}_r \boldsymbol{\Gamma}_r^{-1} \hat{\boldsymbol{K}}_r^T\right) > 0\,,\end{aligned} \tag{9}$$

where the argument (t) is left out for the sake of notational simplicity. It can be shown that $\dot{\mathcal{V}} = -\boldsymbol{e}_s^T \boldsymbol{Q} \boldsymbol{e}_s \leq 0$ for the adaptation law (8), which implies that the adaptive control system is globally stable and thus $\boldsymbol{e}_s(t)$, $\hat{\boldsymbol{K}}_x(t)$ and $\hat{\boldsymbol{K}}_r(t)$ are uniformly bounded. Furthermore, invoking Barbalat's lemma, it can be shown that the state tracking error $\boldsymbol{e}_s(t)$ is *asymptotically stable*, because $\dot{\mathcal{V}}$ is negative semi-definite and uniformly continuous over time. The latter is the result of a bounded $\ddot{\mathcal{V}}$ due to boundedness of $\boldsymbol{e}_s(t)$ and $\boldsymbol{x}_m(t)$ and because the measured signals $\boldsymbol{r}(t)$ are assumed to be bounded. Although $\boldsymbol{e}_s(t)$ is asymptotically stable, it is not guaranteed that $\boldsymbol{K}_x(t) \to \boldsymbol{K}_x^*$ and $\boldsymbol{K}_r(t) \to \boldsymbol{K}_r^*$. This issue has a consequence for the feedback adaptation as will be discussed in Sec. 3.4.

The adaptive algorithm does not impose conditions on the initial values of the gain matrices and it requires no prior knowledge on the dynamic parameters of the feedforward transmission path. This is in contrast to the adaptive algorithms of (Beijen et al., 2018a; Beijen and Hakvoort, 2019).

The adaptation laws in (8) require signals $\boldsymbol{x}_p(t)$, $\boldsymbol{r}(t)$ and $\boldsymbol{e}_s(t)$, which are contaminated with measurement noise. Furthermore, stability and convergence might be affected by parasitic dynamics. These effects are reduced by a *residual noise shaping filter* (NSF in Fig. 2) that adds frequency weighting to the signals by filtering out the unwanted low and high frequency signal content. The NSF is adopted from Beijen et al. (2018a). The NSF is implemented as a 3rd-order Butterworth band-pass filter. The pass-band is related to the performance limitations as discussed in (see Sec. 3.3).

3.3 Performance limits in practice

In theory, the developed MRAC system results in perfect cancellation of floor vibrations ($\mathcal{T}$ is zero) and measured direct disturbances ($\mathcal{C}_s$ is zero), and a highly damped $\mathcal{C}_d(s)$ by a high d_s. However, this performance cannot realised in practice due to several limitations introduced by implementation on the experimental setup, which is detailed in Sec. 4.

Weak integrators Inputs $\boldsymbol{r}(t)$ and $\boldsymbol{x}_p(t)$ of the controller in (5) contain position and velocity of the vibrating floor and payload, see (2). These are reconstructed from the measured accelerations $a_0(t)$ and $a_1(t)$ by integration. Actuator saturation is prevented using weak integrators as proposed by Beijen et al. (2018a). Fifth order weak-integrators with a cut-off at $\alpha = 2 \times 2\pi$ rad/s are used.

Discretisation of the control system The control system is implemented on a discrete control system. The weak integrators of the controller are discretised using the zero-order-hold (ZOH) method. The effect is analysed by assuming a perfect ZOH-filter transfer function with sampling time $t_s = 1/6400\,\mathrm{s}$.

Sensor filtering The experimental setup is equipped with sensor signal conditioners that contain 2^{nd} order Butterworth band-pass filters to suppress sensor noise, parasitic sensor dynamics and aliasing effects. The pass band is $0.1 - 3000\,\mathrm{Hz}$. A similar filter is assumed for the sensor of the actuator force $F_s(t)$.

Actuator dynamics The actuator's induction induces a pole at 331 Hz (Tjepkema, 2012). This dynamics is not included in the plant model, because the pole is well beyond the frequency range of interest.

These effects add parasitic dynamics to the closed loop and thereby limit performance, which unavoidable by the waterbed effect (Beijen et al., 2018b). Fig. 4 shows the effect on $\mathcal{T}(s)$ for a model of the expected dynamics of the experimental setup and the model matching control gains from (7). The weak integrators severely limit the performance of $\mathcal{T}(s)$ below α. The performance beyond α up to the actuator pole is limited by sensor filtering and discretisation to a reduction of -40 dB. The actuator

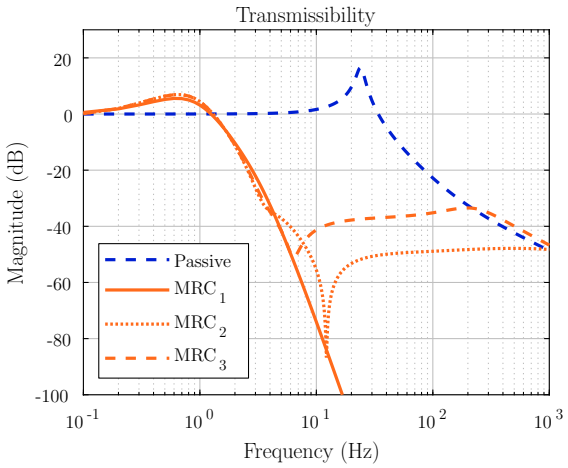

Fig. 4. $\mathcal{T}(s)$ of the modelled vibration isolation system with $m = 3.5\,\mathrm{kg}$, $k = 80\,\mathrm{kN/m}$ and $d = 80\,\mathrm{Ns/m}$ and skyhook damping $d_s = 3580\,\mathrm{Ns/m}$ and model matching control gains. The graphs show the passive and active $\mathcal{T}(s)$ after subsequent addition of weak integrators (MRC_1), sensor filtering and discretisation (MRC_2) and the actuator pole (MRC_3).

dynamics severely limits the performance beyond to the actuator pole. Similarly it can be shown that the weak integrators have no effect on $\mathcal{C}_s(s)$, while the other effects limit performance at high frequencies. The additional dynamics have little effect on $\mathcal{C}_d(s)$. In simulation it is observed that the control gains do not adapt to the model matching values due to the parasitic dynamics. To reduce this effect, the pass-band of the NSF is set to $10 - 100\,\mathrm{Hz}$, being well above the weak-integrator cut-off frequency and below the actuator pole.

3.4 Feedback updating modification

In initial simulation results it was found that the state-tracking error and the feedforward gains $\boldsymbol{K}_r(t)$ converge, but the feedback gains $\boldsymbol{K}_x(t)$ did not converge and high feedback gains are obtained. Note that convergence of the feedback gains was not proven in Sec. 3.2. This result can be explained from the fact that in the reference model all measured disturbances $r(t)$ are perfectly cancelled. In absence of any unmeasured disturbance $w(t)$, the states of the model and real plant match with the correct feedforward gains for any value of k_s and d_s because all states are zero. In other words, these parameters are insufficiently excited. In the presence of any unmeasured disturbance, the states still cannot be matched, because the reference plant is not excited by the unmeasured disturbance and high feedback gains are obtained to reduce the motion of the actual system. In experiments the high feedback gains even result in instabilities due to parasitic high-frequency dynamics.

To circumvent this problem, it is proposed to exploit the physics-based knowledge in the relation between the model-matching feedback and the feedforward gains from (7). The feedback gain is kept zero, except for the second element, which is updated each time step using the desired skyhook damping minus the second element of the feedforward gain.

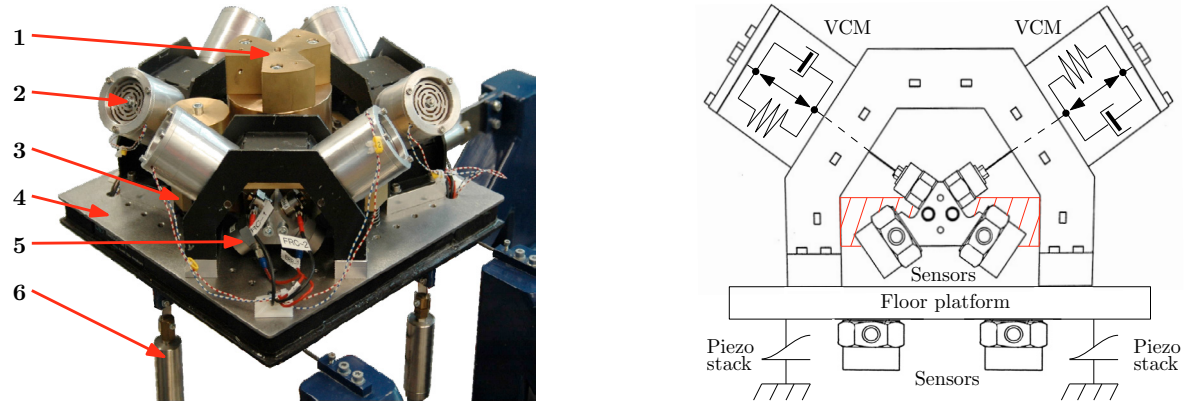

(a) (b)

Fig. 5. (a) Experimental setup (Tjepkema (2012)), with; (1) payload; (2) voice coil motors (VCMs); (3) payload platform; (4) floor platform; (5) payload accelerometers; and (6) piezo stacks. The floor accelerometers, located underneath (4), are not visible. (b) Schematic picture with the payload platform in read. Also the floor sensors are visible.

4. RESULTS

The proposed MRAC scheme is validated on the experimental setup shown in Fig. 5a. The payload is connected by wire flexures to six voice coil motors (VCMs) in a Stewart platform configuration. Elastic element provide linear guidance of the VCMs. This elastic suspension introduces eigenfrequencies between 15 and 45 Hz as measured an modelled by Tjepkema (2012). The Stewart platform is mounted on a floor platform that can be excited by three piezo stacks. Six accelerometers placed on the payload and six accelerometers placed on the floor platform. The control system is implemented on a dSPACE system running at a sampling frequency of $f_s = 6400$ Hz. No disturbance forces $F_s(t)$ are measured. Unmeasured disturbance forces $F_d(t)$ due to acoustics and cabling are considered negligible. The acceleration signals are fed through the earlier mentioned signal conditioners before entering the control system. Only motion in the vertical direction is considered in this paper.

The reference model parameters are selected as proposed in Sec. 2.2 with skyhook damping set to $d_s = 3580$ Ns/m. $\boldsymbol{Q} = \text{diag}(4.75 \times 10^4, 2.2 \times 10^3)$ such that $\bar{\boldsymbol{P}} \approx [1, 1]^T$ for the expected plant parameters. The adaptation gain matrix of the feedforward path is defined by $\boldsymbol{\Gamma}_r = \text{diag}\left(1 \times 10^{15}, 6 \times 10^{10}, 0\right)$. The third entry is not adapted because no disturbance forces are measured. These values are chosen to get an acceptable convergence rate of $\boldsymbol{K}_r(t)$ according to (8) for the expected size of the parameters and signals and some tuning. The feedback gain $\boldsymbol{K}_x(t)$ is updated indirectly as proposed in Sec. 3.4. The first two entries of $\boldsymbol{K}_r(t)$ are initially set to zero. Three filtered pseudo-binary-random-sequence (PRBS) signals are fed to the piezo stacks to approximately provide the ASML floor vibration specification of an industrial environment with $10^{-7}\,(\text{m/s}^2)^2/\text{Hz}$ at low frequencies and $10^{-8}\,(\text{m/s}^2)^2/\text{Hz}$ at high frequencies (Schmidt et al., 2014).

Fig. 6 shows the adaptation of the first two components of the feedforward gain $\boldsymbol{K}_r(t)$. Note the third component is not updated and the feedback gain is updated indirectly. The parameters converge in approximately 20 s.

Fig. 7 shows the transmissibility plot obtained from experiments with control gains fixed after convergence. A broad banded reduction of $\mathcal{T}$ up to -40 dB is visible between 5 and 100 Hz, which is in line with the expectation in Fig. 4. This corresponds to a reduction of the acceleration levels of 100 times with respect to the passive system. Below 5 Hz and above 200 Hz the MRAC controlled system is outperformed by the passive system by the weak integrators and actuator poles respectively.

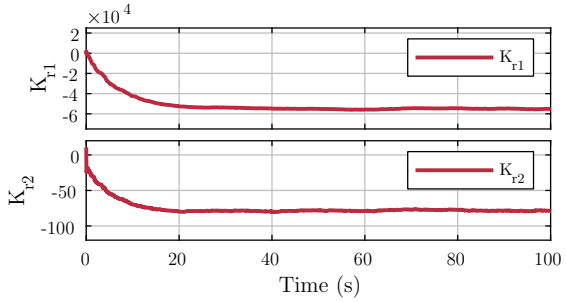

Fig. 6. Adaptation of $K_{r,1}(t)$ and $K_{r,2}(t)$.

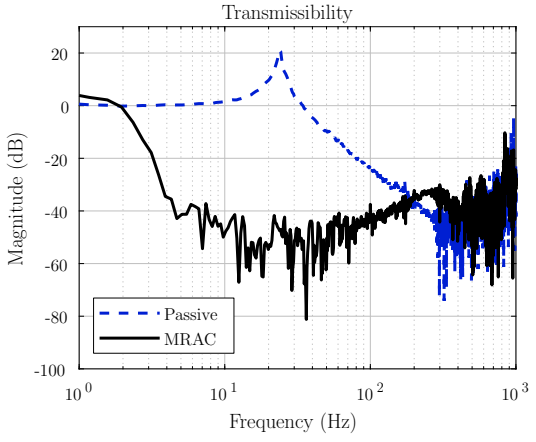

Fig. 7. Measured transmissibility in vertical direction of the experimental setup. The blue dashed line shows the passive transmissibility, and the black solid line the active transmissibility.

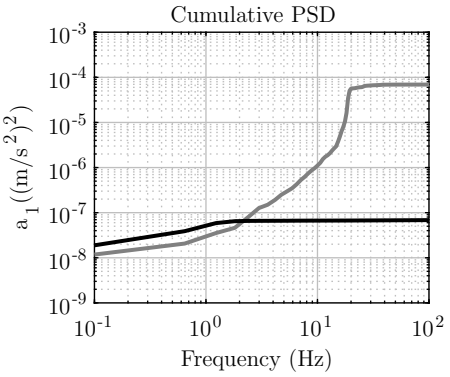

Fig. 8. Measured cumulative PSD of the payload acceleration for the passive (grey) and active (black) system.

Fig. 8 shows the measured cumulative PSD from 0.1 Hz of the payload acceleration for the passive and MRAC controlled system. Compared to the passive system, a significant performance improvement is visible beyond 2 Hz when MRAC is applied. The increased power up to 2 Hz is due to the weak integrators of the controller. The cumulative root-mean-square (RMS) acceleration up to 100 Hz is found to be $\mathrm{RMS_p} = 8.32 \times 10^{-3}\,\mathrm{m/s^2}$, for the passive system and $\mathrm{RMS_a} = 2.62 \times 10^{-4}\,\mathrm{m/s^2}$ for the MRAC controlled system. The RMS acceleration level in the frequency band of interest is thus reduced 32 times.

5. CONCLUSIONS

This paper presents a model reference adaptive control (MRAC) strategy to achieve broad banded vibration isolation. A reference model is proposed with skyhook damping and no effect of the measured disturbances. The model matching controller is a disturbance feedforward controller with skyhook feedback damping. The control gains only depend on the stiffness and damping of the support. A Lyapunov based adaptive algorithm simultaneously updates the feedforward and feedback controller and ensures state matching and bounded parameters. No prior knowledge on the stiffness and damping of the support is needed. The feedback parameters does not converge due to insufficient excitation. Based on physical insight, the feedback gains are updated using the adapting feedforward gains, which are excited by the floor vibrations. The MRAC system is validated experimentally on a hard mount isolation system. A reduction up to -40 dB is observed for frequencies between 5 and 100 Hz. Furthermore, the root-mean-square (RMS) acceleration of the MRAC controlled system is 32 times lower than the passive RMS acceleration in the $0.1 - 100$ Hz band.

Future work will investigate the observation that internal modes of the payload do not affect convergence and performance. Furthermore the extension to more degrees of freedom will be considered. Further investigation will also consider how to combine the well-defined convergence rate of RLS (Beijen and Hakvoort, 2019) without the need to know the secondary path as with MRAC.

REFERENCES

Alleyne, A. and Hedrick, J.K. (1995). Nonlinear adaptive control of active suspensions. *IEEE transactions on control systems technology*, 3(1), 94–101.

Åström, K.J. and Wittenmark, B. (2013). *Adaptive control*. Courier Corporation.

Beijen, M. and Hakvoort, W. (2019). Filtered-error recursive least squares optimization for disturbance feedforward control in active vibration isolation. *IFAC-PapersOnLine*, 52(15), 448 – 453. 8th IFAC Symposium on Mechatronic Systems 2019.

Beijen, M., Heertjes, M., Van Dijk, J., and Hakvoort, W. (2018a). Self-tuning mimo disturbance feedforward control for active hard-mounted vibration isolators. *Control engineering practice*, 72, 90–103.

Beijen, M., Cong, B., and Heertjes, M. (2018b). Design and performance tradeoffs in mimo disturbance feedforward control. In *2018 IEEE 15th International Workshop on Advanced Motion Control (AMC)*, 443–448. IEEE.

Fuller, C.C., Elliott, S., and Nelson, P.A. (1996). *Active control of vibration*. Academic Press.

Heertjes, M., de Graaff, K., and van der Toorn, J.G. (2005). Active vibration isolation of metrology frames; a modal decoupled control design. *Journal of Vibration and Acoustics*, 127(3), 223–233.

Karnopp, D. (1995). Active and semi-active vibration isolation. In *Current Advances in Mechanical Design and Production VI*, 409–423. Elsevier.

Khalil, H.K. and Grizzle, J.W. (2002). *Nonlinear systems*, volume 3. Prentice hall Upper Saddle River, NJ.

Landau, I. (1974). A survey of model reference adaptive techniques - theory and applications. *Automatica*, 10(4), 353–379.

Preumont, A., Horodinca, M., Romanescu, I., De Marneffe, B., Avraam, M., Deraemaeker, A., Bossens, F., and Hanieh, A.A. (2007). A six-axis single-stage active vibration isolator based on stewart platform. *Journal of sound and vibration*, 300(3-5), 644–661.

Rivin, E.I. (2003). *Passive vibration isolation*. Amer Society of Mechanical.

Schmidt, R.M., Schitter, G., and Rankers, A. (2014). *The Design of High Performance Mechatronics-: High-Tech Functionality by Multidisciplinary System Integration*. Ios Press.

Tjepkema, D. (2012). *Active hard mount vibration isolation for precision equipment*. phdthesis, University of Twente, Enschede, The Netherlands.

van der Poel, T., van Dijk, J., Jonker, B., and Soemers, H. (2007). Improving the vibration isolation performance of hard mounts for precision equipment. In *2007 IEEE/ASME international conference on advanced intelligent mechatronics*, 1–5. IEEE.

Wang, Y.P. and Sinha, A. (1997). Adaptive sliding mode control algorithm for a multi-degree-of-freedom microgravity isolation system. In *Proceedings of the 1997 IEEE International Conference on Control Applications*, 797–802. IEEE.

Wesselink, J. and Berkhoff, A.P. (2008). Fast affine projections and the regularized modified filtered-error algorithm in multichannel active noise control. *The Journal of the Acoustical Society of America*, 124(2), 949–960.

Zuo, L., Slotine, J.J., and Nayfeh, S.A. (2005). Model reaching adaptive control for vibration isolation. *IEEE Transactions on Control Systems Technology*, 13(4), 611–617.